Prepublished copy

Nature Environment & Pollution Technology

This is a peer-reviewed prepublished version of the paper to be published in Vol. 25, No. 4, December 2026 issue

Original Research

Hydrodynamic Enhancement of Direct Contact Membrane Distillation Using a Corrugated Feed Channel: A Numerical Study

Fajer M. Alelaj[1]†, Mansour Ahmed[1], Hussain Al-Sairfi[1], Garudachari Bhadrachari[1], Shimaa Zahran[2] and Mohamed R. Elmarghany[2,3]

[1]Department of Water Research Center, Kuwait Institute for Scientific Research (KISR), Kuwait

[2]Mechanical Power Engineering Department, Faculty of Engineering, Mansoura University, Egypt

[3]Research and Development Department, SHARQAWI air distribution systems factory, Jeddah, Saudi Arabia

†Corresponding author: Fajer M. Alelaj; Dr.Fajer.Alelaj@gmail.com

ORCID ID of Author: Fajer M. Alelaj https://orcid.org/0009-0009-2364-0805

Key Words	Direct contact membrane distillation, Hydrodynamic enhancement, Permeate flux, Rib geometry
DOI	https://doi.org/10.46488/NEPT.2026.v25i04.D1922 (DOI will be active only after the final publication of the paper)
Citation for the Paper	Alelaj, F. M., Ahmed, M., Al-Sairfi, H., Bhadrachari, G., Zahran, S. and Elmarghany, M. R., 2026. Hydrodynamic enhancement of direct contact membrane distillation using a corrugated feed channel: A numerical study. *Nature Environment and Pollution Technology*, 25(4), D1922. https://doi.org/10.46488/NEPT.2026.v25i04. D1922

ABSTRACT

A numerical simulation of a direct contact membrane distillation (DCMD) cell withrectangular corrugations placed in the feed channel was studied in this research to investigate the influence of corrugated feed-channel geometry on hydrodynamic behavior and permeate flux in DCMD systems. The coupling of flow and mass transfer in channel ,geometries both in conventional and modified ,geometries was simulated in a two-dimensional steady-state model to simultaneously describe mass transfer and flow. The effect of different rib height, ,breadth and pitch on pressure drop and permeate flow was investigated in a systematic manner. The findingsalso indicated that rib geometry is a critical factor in determining mass transfer effectiveness and flow patterns. Specifically, raising the rib height by 1mm to 3mm resulted in a significant reduction in permeate flux, mainly due to the growth of a greater number of layers of obstruction of the flow and the formation of layers of concentration. On the same note, permeate flux reduced gradually with an increase in rib breadth. On the other hand, an increase of rib pitch 5mm by 15mm provided a small improvement in flux enhancement by removing excessive blockage of flows but also keeping mix

levels satisfactory. The pressure-drop analysis has shown that smaller rib pitches increased hydraulic resistance, which points to the fact that there is a trade-off between increased mass transfer and decreased flow losses. In general, the best setup was achieved with low rib height, intermediate ,width and increased pitch, which optimally balanced the augmentation of flux and minimum pressure loss. The results provide useful insight into the influence of rib geometry on mass-transfer behavior and hydraulic performance in DCMD modules. The study demonstrates that geometric optimization of corrugated channels is necessary to balance flow disturbance and hydraulic resistance in DCMD systems.

INTRODUCTION

The problem of freshwater scarcity is getting too vital to be overlooked in modern society, especially in the Gulf region, where the growing population, industrialisation, and climate change have started to merge to cause the issue (Sherif et al., 2023; Salman et al., 2025). This has led to the fact that desalination technologies have become necessary for securing a sustainable water supply, particularly in dry and semi-arid regions (Al-masoudi, and Jamoussi, 2024; Al-Sairfi et al., 2026). Membrane distillation (MD) is an effective thermally driven separation process, designed at relatively low temperature, with low-grade and renewable heat input, and having high salt rejection (Soumbati et al., 2025; Drioli, Ali and Macedonio, 2015).

A microporous hydrophobic membrane divides a hot saline feed with a chilled ,permeate allowing only water vapour to go through the network of pores (Nthunya, and Mamba, 2025). Vapour transport is motivated by the pressure gradient between the vapour and the ,liquid brought about by the temperature difference across the membrane. Although it has many benefits, the commercial application of MD is still very limited because ofrelatively low permeate flux and thermal efficiency compared with traditional desalination methods (Gobran et al., 2025; Zaragoza et al., 2018). All these deficiencies can mainlybe attributed to polarisation of temperature and concentration and heat losses in the membrane module (Suleman, Asif and Jamal, 2021).

Among the MD configurations, direct contact membrane distillation (DCMD) is also explicitly studied due to its simplicity and easy implementation (Sheikh et al., 2025; Qasim et al., 2021). Hot saline feed and cold permeate streams in DCMD are introduced to contact opposite membrane ,surfaces and the temperature gradient created causes a vapour-pressure difference across the membrane. DCMD has lower mass-transfer resistance and greater vapour flux compared with air-gap, vacuum, and sweeping-gas MD variants (Francis, Ahmed and Hilal, 2022; Boubakri et al., 2017). However, its thermal performance is limited by large amounts of conductive heat losses across the membrane and temperature polarisation, which reduces the driving force across the va-pours (Jing, et al., 2025). Hence, the DCMD cell design optimisation is essential to increase performance and make the technology a significant step to be deployed on a large scale (Cancilla et al., 2026).

The literature on previous membrane distillation has been more concerned with the use of materials and the optimisation of operations to enhance performance (Farid, et al., 2024; Xu, Zhu, and Li, 2022). The fabri-cation of hydrophobic polymer membranes, surface functionalisation, and pore-structure engineering have all

produced significant gains in vapour flux and wetting resistance. At the same time, there have been a large number of experimental and numerical studies on the effect of operating parameters (feed temperature, salinity, flow velocity, and membrane thickness) on the heat and mass transfer behavior in DCMD systems (Hu et al., 2025; Lou et al., 2019). Regularly, these studies have found the polarisation of temperatures and conductive heat losses across the membrane to be the major constraints affecting overall productivity and thermal efficiency. Researchers have used turbulence promoters, spacers, and corrugated flow channels to alleviate these effects and increase convective heat transfer while decreasing the boundary-layer thickness (Taamneh, and Bataineh, 2017; Swaidan et al., 2024).

The current study investigates the influence of corrugated feed-channel geometry on the hydrodynamic and mass-transfer behavior of a DCMD system under different geometric conditions. A numerical model is built to examine the heat and mass transport processes in the redesigned cell and compare their impact on the vapour-flux, temperature polarisation coefficient, and the overall thermal efficiency. The behavior of the modified design is compared with that of a traditional membrane cell under the same conditions systematically. Parametric experiments test the effectiveness of feed temperature, salinity, flow velocity, and membrane parameters on system performance.

The remainder of the paper is organized as follows: Section 2 discusses the mathematical model; Section 3 studies the Mesh Dependency Test; Section 4 provides the results and discussion and determines the effect of rib height, rib width, and rib pitch on the hydrodynamic features; and Section 5 concludes the paper and summarizes the key findings.

2. MATHEMATICAL MODEL

2.1 Physical Description

To investigate the effect of mass transfer in conventional and modified membrane cells, a two-dimensional, steady-state model of DCMD has been formulated. The computational domain is divided into 3 regions: the hot saline feed channel, the hydrophobic micro-porous membrane, and the cold permeate channel. The membrane serves to separate the two streams of fluid to allow only vapour to penetrate and to exclude the intrusion of liquid, since the membrane is hydrophobic.

The standard flat-plate DCMD cell has been adapted by adding a corrugated feed channel to increase productivity, reduce salt concentration, and reduce temperature polarization. The corrugations are arranged into rectangles and set at fixed positions on the wall of the feed channel close to the membrane surface, thereby creating a structured flow channel that favors disturbance and flow disruption of the boundary flow. The geometry of corrugation is characterized by height, width, and pitch, and all these parameters are systematically altered to determine the effect of each one on hydrodynamic performance (Sherif et al., 2023) . Besides, the overall feed-channel height is also a design parameter used to examine its effect on the temperature polarization

and vapour flux (Elhenawy et al., 2020; Darman, Niknafs and Jalali, 2023). The given parametric design methodology allows a thorough evaluation of the influence of structural changes at the cell level on the functioning of membrane distillation and provides effective suggestions that could be used to improve the design of DCMD modules.

The schematic drawing of the proposed DCMD cell given in Fig. 1 includes the hot feed channel, hydrophobic membrane and cold permeate channel. The adjusted design has corrugations in rectangular form with different widths, heights, and pitches on the feed channel wall near the membrane. The selected rib dimensions were chosen based on practical manufacturability constraints and previous corrugated-channel studies reported in the literature. Excessively large ribs may cause severe channel blockage and unstable flow behavior, while very small ribs produce negligible hydrodynamic disturbance.

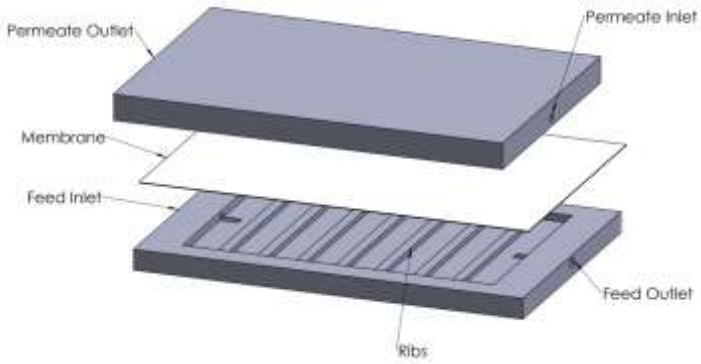

Fig. 1: schematic diagram of the proposed cell.

The computational calculations were conducted at an inlet velocity of 0.01 m/s, with the feed and permeate inlet temperatures held at 343 K and 293 K, respectively. The geometric characteristics of the ribs were systematically varied to evaluate their influence on thermal and flow behavior, with rib heights ranging from 1 to 3 mm, rib widths from 2 to 4 mm, and rib pitches (spacing between successive ribs) from 5 to 15 mm.

2.2 Governing Equations

The transport phenomena in the feed and permeate channels are described by the steady-state incompressible Navier–Stokes, energy, and species conservation equations (Qtaishat et al., 2008).

Continuity

$$\nabla \cdot \mathbf{u} = 0 \tag{1}$$

Momentum

$$\rho(\mathbf{u} \cdot \nabla)\mathbf{u} = -\nabla p + \mu \nabla^2 \mathbf{u} \tag{2}$$

Energy

$$\rho c_p(\mathbf{u} \cdot \nabla)T = k\nabla^2 T \quad (3)$$

2.3 Vapor Transport Through the Membrane

The vapor flux across the membrane is governed by the vapor pressure difference across the membrane surfaces which can be represented as follow:

$$J = C_m\left(P_{v,f} - P_{v,p}\right) \quad (4)$$

where C_m is the membrane mass transfer coefficient and $P_{v,f}, P_{v,p}$ are the vapor pressures at the feed and permeate membrane surfaces which can be calculated using Antoine equation (Lee, 2025) .

The membrane mass transfer coefficient is expressed as:

$$C_m = \left(\frac{1}{C_K} + \frac{1}{C_M}\right)^{-1} \quad (5)$$

where C_K and C_M are the Knudsen and molecular diffusion coefficients.

In this study, the numerical model was established based on several simplifying assumptions. The flow was assumed to be steady-state, two-dimensional, laminar, and incompressible, with constant thermophysical properties throughout the domain. Membrane wetting was neglected, and complete salt rejection was considered. Moreover, water vapor within the membrane pores was assumed to obey the ideal gas law, and local thermal equilibrium was maintained at the membrane interfaces.

2.4 Boundary Conditions and Numerical Procedure

At the feed-channel inlet, a uniform velocity profile of 0.01 m/s and a temperature of 343 K were imposed. The permeate inlet temperature was fixed at 293 K. Atmospheric pressure boundary conditions were applied at both outlet boundaries. No-slip velocity conditions were imposed at all solid walls. The membrane was considered hydrophobic and non-wetted, with complete salt rejection. Heat transfer through the membrane included both conductive and latent heat transport mechanisms. The membrane surfaces were thermally coupled with the adjacent fluid domains. The governing equations were solved using the finite volume method in ANSYS Fluent. Pressure velocity coupling was achieved using the SIMPLE algorithm. Second-order upwind discretization schemes were applied to the momentum and energy equations to improve numerical accuracy. The convergence criterion for all governing equations was set to 10^{-6} for the continuity, momentum, and energy residuals. Simulations continued until stable values of permeate flux and the temperature distribution were achieved. Table 1 demonstrated the membrane and operating parameters.

Table 1: Membrane and operating parameters.

Parameter	Value
Membrane thickness	0.12 mm
Membrane porosity	0.75
Membrane tortuosity	2.0833
Mean pore size	0.22 μm
Feed inlet temperature	343 K
Permeate inlet temperature	293 K
Feed velocity	0.01 m/s
Membrane material	PVDF

3. MESH DEPENDENCY TEST

A mesh dependency test was performed in ANSYS by progressively increasing the number of elements until a quantitative convergence criterion was achieved. A finer mesh was utilized at the corners to enhance the resolution of boundary layers and accurately capture the steep temperature and velocity gradients, resulting in increased simulation accuracy. The relative error of key output parameters, including permeate flux and temperature distribution, was evaluated between successive mesh refinements, and the final mesh was selected when the relative error dropped below 1% at 38945 elements. Fig. 2 (a) shows the computational domain and mesh, respectively, and Fig. 2 (b) shows the variation of relative error with increasing number of elements.

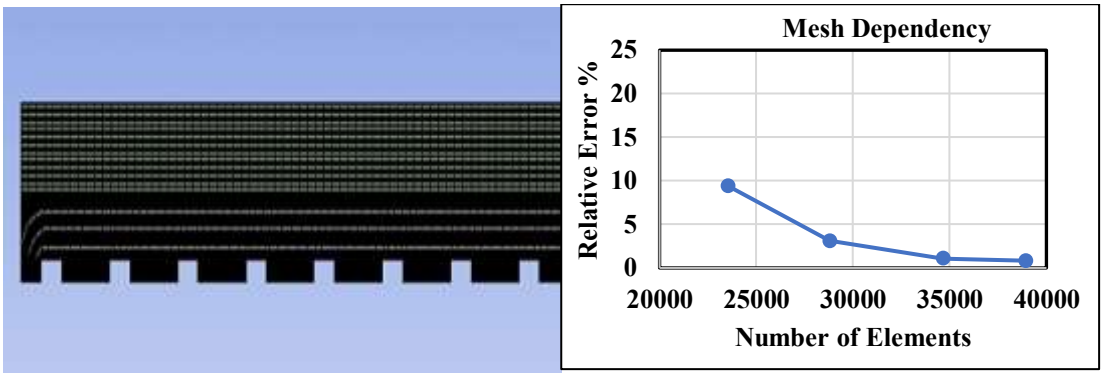

(a) (b)

Fig. 2: (a) shows the computational domain and mesh, respectively, and Figure 2 (b) shows the variation of relative error with increasing number of elements.

The final computational mesh was selected after achieving a relative error below 1%, thereby minimizing numerical uncertainty in the predicted permeate flux results.

3.1 Model Validation

To validate the developed numerical model, the predicted permeate flux values were compared with previously published numerical and experimental DCMD studies available in the literature. The comparison was conducted under similar operating conditions, including feed and permeate temperatures, membrane characteristics, and flow configuration. Table 2 presents the comparison between the present numerical model and the published results reported by Qtaishat et al. (2008) and Lou et al. (2019). The comparison demonstrates good agreement between the current simulation and the literature data, with deviations within an acceptable range for CFD-based DCMD investigations. This confirms the capability of the present model to accurately predict the coupled heat and mass transfer behavior in direct contact membrane distillation systems.

Table 2: Validation of the present numerical model with published literature

Study	Method	Permeate Flux (kg/m²·h)
Qtaishat et al. (2008)	Numerical	14.9
Lou et al. (2019)	CFD simulation	15.2
Present study	Numerical simulation	15.4

The maximum deviation between the present model and the literature results was below 4%, indicating satisfactory agreement and confirming the reliability of the numerical methodology used in this study.

4. RESULTS AND DISCUSSION

A parametric study was conducted to determine the effect of rib height, rib width, and rib pitch on the hydrodynamic features and membrane flux of the modified cell. The performance of the corrugated feed-channel configurations was evaluated relative to the conventional flat-channel DCMD configuration under the same operating conditions. All simulations were performed under identical inlet operating conditions to isolate the influence of geometric parameters on the hydrodynamic and mass-transfer behavior of the DCMD system.

4.1 Effect of rib height

The dependence between permeate flux and rib height is shown in Fig. 3 and the pitch and width of the rib are kept constant (15mm and 4mm, respectively). The outcomes illustrate an evident pattern: the higher the rib height, the lower the permeate flux. The ribs at a rib height of 1 mm and a thickness are successful in causing perturbation to the flow, which improves the mixing in the region of the membrane surface, as well as in the mitigation of concentration polarization, without the ribs greatly hindering the flow. On the other hand, raising rib height enhances blockage in the channel leading to larger recirculation zones and lesser effective cross-sectional area of flow. This change decreases the total fluid velocity and residence time in areas where the convective transport is less efficient, and promotes the development of thicker concentration boundary layers in places near the membrane. This will cause the mass transfer driving force to reduce, resulting in reduced permeate flux at high rib height. Therefore, the results of this study highlight the importance of having small enough rib heights to facilitate the exchange of mass in spite of the increase in surface roughness and are therefore relevant to the fact that ribs have to be optimized in size, as opposed to increased size. Although flow disturbance generated by the corrugated structures may improve local mixing near the membrane surface, excessive rib height increases channel blockage and weakens overall mass-transfer performance.

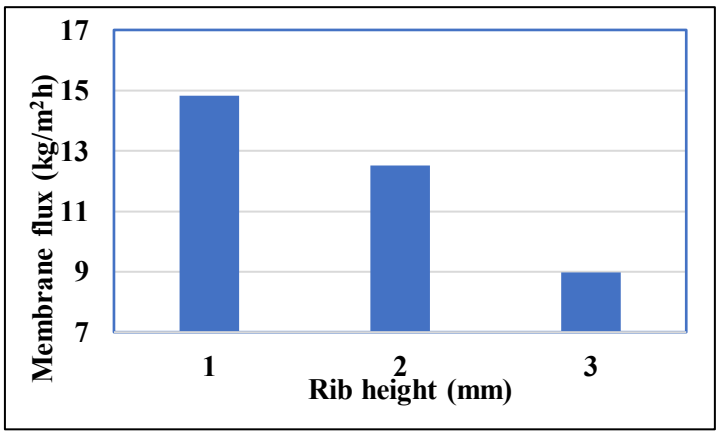

Fig. 3: Effect of rib height on permeate flux at fixed rib width = 4 mm and rib pitch = 15 mm.

4.2 Effect of rib width

Fig. 4 shows the variation of permeate flux with rib width, with rib height and pitch remaining constant at 1mm and 15mm respectively. The data indicate a constant reduction in permeate flux with the increase in the rib width between 2 and 4mm. In particular, the flux is about 15.4 kg/m²·h at a rib width of 2 mm, 15.1 kg/m²·h at 3 mm, and 14.8 kg/m²·h at 4 mm. This tendency can be explained by the fact that narrower ribs take up less space in the channel; as such, the channel can have higher local fluid velocities and stronger shear forces in the proximity of the membrane surface. These conditions increase mixing and reduce concentration polarization. Increase in rib width, on the other hand, causes increased channel blockage of the channel and reduces near-wall convection, stimulating the formation of thicker concentration boundary layers. This, in turn, enhances the resistance to mass transfer and leads to low permeate flux. In general, these results point to the fact that the presence of ribs is beneficial to facilitate the occurrence of a flow disturbance, but very broad ribs may hamper the process of mass transfer by limiting the effective development of the flow around the membrane surface. As such, the width of the ribs should be optimized to achieve maximum filtration. These findings indicate that corrugation geometry does not necessarily guarantee flux enhancement, and improper rib dimensions may negatively affect mass-transfer efficiency.

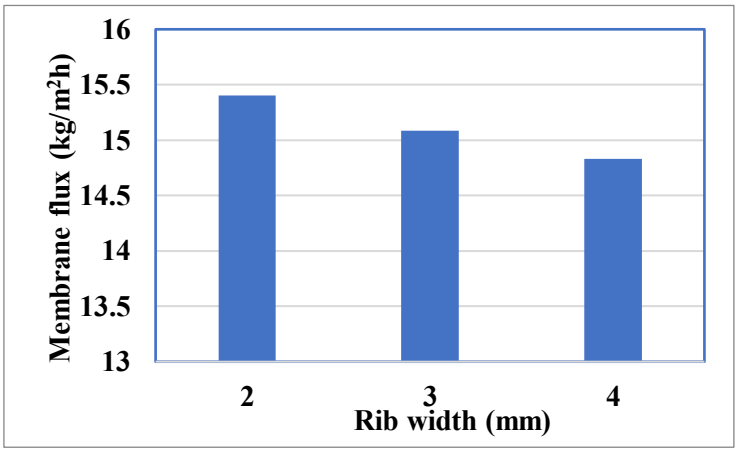

Fig. 4: Effect of rib width on permeate flux at fixed rib height = 1 mm and rib pitch = 15 mm.

4.3 Effect of rib pitch

Fig. 5 shows the effect of differences in rib distance (rib pitch) on permeate flux, with rib width and height maintained at 2 mm and 1 mm, respectively. The results indicate that permeate flux gradually increases with the rise in rib pitch between 5mm and 15mm. Particularly, the flux increases to 15.1 kg/m²·h and 15.2 kg/m²·h at 5 and 10 mm, respectively, and to 15.4 kg/m²·h at 15 mm. In the case of close pitch (ribs), more obstacles are introduced to the flow, resulting in larger swirling areas between the ribs. Although mixing close to the membrane can be made more effective, over-obstruction reduces flow close to the membrane surface and lessens the passage of materials across it. The higher the rib pitch, the less restricted the channel, and the more fluid can

flow freely while still creating enough disturbance to break up concentration boundary layers. This enhanced mixing/flow resistance ratio increases mass transfer, leading to a higher permeate flux at larger rib pitched. Therefore, the results show the significance of rib spacing optimization to obtain the maximum flux without imposing any unwarranted flow resistance and energy loss.

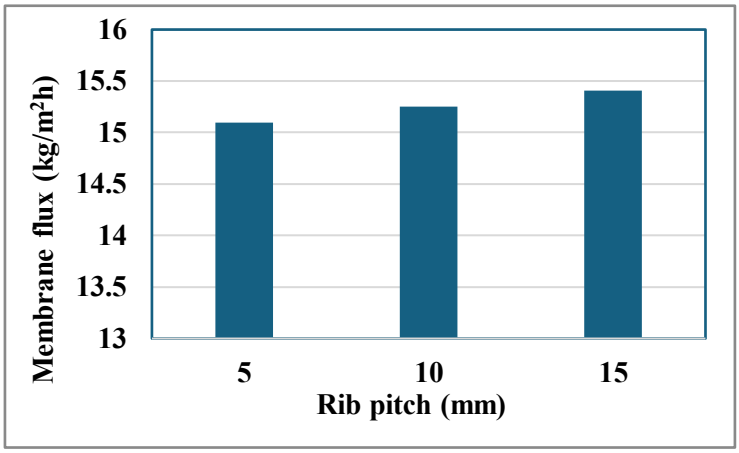

Fig. 5: Effect of rib pitch on permeate flux at fixed rib height = 1 mm and rib width = 2 mm.

4.4 Effect of rib dimensions on pressure drop

Table 3 is a summary of the shape and arrangement of ribs on pressure drop across the feed channel. The results show that pressure drop decreases steadily with increasing rib pitch, regardless of rib width. Closer ribs increase flow resistance. For instance, with 1 mm high and 2 mm wide ribs, the pressure drop decreases from 0.803 Pa at a 5 mm pitch to 0.625 Pa at a 15 mm pitch. The same trends are observed in terms of ribs with 3 mm width and 4 mm width, which supports the concept that the spacing between ribs is more obstructive and results in more losses related to friction. The effect of rib width, however, is more subtle. With a small pitch of 5mm, a slight change in pressure drop occurs as the widening of rib by 3mm to 4mm, resulting in a decrease in pressure drop. However, larger pitches usually cause greater pressure drops due to broader ribs that tend to interrupt a greater portion of the passageway. On the whole, these findings suggest that rib pitch is the major factor affecting the loss of pressure, and that the role of rib width is also significant, but secondary, which is conditional upon the adjacency of ribs. The results demonstrate that the increase in permeate flux must be balanced against the additional hydraulic resistance introduced by corrugated structures. Therefore, an optimal rib configuration should simultaneously maximize mass transfer while minimizing pressure losses and pumping power requirements.

Table 3: Pressure drop at the feeding side of the DCMD cell.

		ΔP (Pa)		
Height (mm)	**Width (mm)**	**Pitch = 5mm**	**Pitch = 10 mm**	**Pitch = 15 mm**
1	2	0.802928	0.7635086	0.6253983
	3	0.822953	0.7731061	0.6513754
	4	0.7866656	0.763927	0.705921

Overall, the results suggest that rib geometry influences not only hydrodynamic behavior and permeate flux, but also the local thermal transport characteristics and temperature polarization phenomena within the DCMD module**.**

5. CONCLUSIONS

The current study has investigated a corrugated feed channel using numerical simulations in order to identify the effect of its geometric properties on mass transfer and fluid dynamics of a direct contact membrane distillation (DCMD) system. The numerical results indicate that the hydrodynamic effect of corrugated channels strongly depends on rib geometry, where both beneficial mixing effects and adverse flow obstruction mechanisms coexist. The results clearly suggest that both permeate flux and hydraulic resistance are highly influenced by the morphology and the dimensions of the ribs. The most significant of the investigated parameters was the rib height: the elevation of the rib height by 1mm to 3mm led to a strong reduction in the permeate flux, mainly because of the increased channel blockage and the formation of additional, thicker layers of concentration boundary near the membrane surface. Rib width also had a significant influence, as permeate flux decreased from 15.4 to about 14.8 kg/m²·h due to an increase of rib width to 4mm. Conversely, by increasing the rib pitch to 15mm this led to a small flux improvement, with the flux increasing from 15.1 to about 15.4 kg/m²·h as the flow encountered less obstruction while still benefiting from adequate mixing.

It was also observed that the pressure drop across the channel reduced to almost 0.80 Pa to almost 0.63 Pa as a result of increased spacing between ribs, which supports the argument that closely spaced ribs increase hydraulic resistance. The above observations highlight the paramount importance of striking a balance between the extra energy needed to overcome the resistance to flow versus the gains of improving mass transfer. Among the investigated configurations, the case with a rib height of 1 mm, rib width of 2 mm, and rib pitch of 15 mm provided the most balanced performance in terms of permeate flux and pressure drop within the investigated operating conditions. Therefore, channel corrugation should be carefully optimized to achieve performance enhancement without introducing excessive hydraulic resistance or flow blockage. On the whole, all these findings prove the fact that under the influence of even the slightest changes in the channel geometry, the system can be significantly affected and can be useful in designing DCMD modules that will be more efficient without involving complicated structural changes.

Author Contributions: Conceptualization, F.M.A., M.A. and H.A.; methodology, F.M.A. and G.A.; software, G.A.; validation, M.A., H.A. and S.Z.; formal analysis, F.M.A., M.R.E. and S.Z.; investigation, M.R.E., M.A. and H.A.; resources, G.A. and M.R.E.; data curation, S.Z.; writing original draft preparation, F.M.A.; review and editing, M.A., H.A. and M.R.E.; visualization, G.A. and S.Z.; supervision, M.R.E.; project administration, M.R.E.; funding acquisition, F.M.A, H.A.. All authors have read and agreed to the published version of the manuscript.

Funding: This research received no external funding.

Institutional Review Board Statement: Not applicable.

Informed Consent Statement: Not applicable.

Conflicts of Interest: The authors declare no conflicts of interest.

REFERENCES

Alkhudhiri, A., Darwish, N. and Hilal, N. (2012) 'Membrane distillation: A comprehensive review', *Desalination*, 287, pp. 2–18. doi:10.1016/j.desal.2011.08.027.

Alklaibi, A.M. and Lior, N. (2005) 'Membrane-distillation desalination: Status and potential', *Desalination*, 171(2), pp. 111–131. doi:10.1016/j.desal.2004.03.024.

Almasoudi, S. and Jamoussi, B. (2024) 'Desalination technologies and their environmental impacts: A review', *Sustainable Chemistry One World*, 1, p. 100002. doi:10.1016/j.scowo.2024.100002.

Al-Sairfi, H., Koshuriyan, M. and Ahmed, M. (2023) 'Performance feasibility study of direct contact membrane distillation systems in the treatment of seawater and oilfield-produced brine: The effect of hot- and cold-channel depth', *Desalination and Water Treatment*, 313, pp. 26–36. doi:10.5004/dwt.2023.29942.

Al-Sairfi, H., Salman, M., Al-Foudari, Y. and Ahmed, M. (2026) 'Modeling the influence of ionic strength on mineral solubility in concentrated brine solutions', *Processes*, 14(1), p. 172. doi:10.3390/pr14010172.

Boubakri, A., Hafiane, A. and Bouguecha, S.A.T. (2017) 'Direct contact membrane distillation: Capability to desalt raw water', *Arabian Journal of Chemistry*, 10, pp. S3475–S3481. doi:10.1016/j.arabjc.2014.02.010.

Bou-Rabee, M.A., Alelaj, F.M. and Al-Sairfi, H. (2025) 'Quantifying the economic loss and operational implications of air pollution on grid-connected PV systems in the Arabian Peninsula: A machine learning-based analysis', *IEEE Access*, 14, pp. 4180–4188. Available at: https://ieeexplore.ieee.org/abstract/document/11318572

Cancilla, N., Cipollina, A., Gurreri, L. and Ciofalo, M. (2026) 'Direct contact membrane distillation: A critical review of transmembrane heat and mass transfer models', *Membranes*, 16(2), p. 64. doi:10.3390/membranes16020064.

Darman, M., Niknafs, N. and Jalali, A. (2023) 'Effect of wavy corrugations on the performance enhancement of direct contact membrane distillation modules: A numerical study', *Chemical Engineering and Processing: Process Intensification*, 190, p. 109421. doi:10.1016/j.cep.2023.109421.

Drioli, E., Ali, A. and Macedonio, F. (2015) 'Membrane distillation: Recent developments and perspectives', *Desalination*, 356, pp. 56–84. doi:10.1016/j.desal.2014.10.028.

Elhenawy, Y., Elminshawy, N.A., Bassyouni, M., Alanezi, A.A. and Drioli, E. (2020) 'Experimental and theoretical investigation of a new air gap membrane distillation module with a corrugated feed channel', *Journal of Membrane Science*, 594, p. 117461. doi:10.1016/j.memsci.2019.117461.

Farid, M.U. *et al.* (2024) 'Advancements in nanoenabled membrane distillation for a sustainable water–energy–environment nexus', *Advanced Materials*, 36(17), p. 2307950. doi:10.1002/adma.202307950.

Francis, L., Ahmed, F.E. and Hilal, N. (2022) 'Advances in membrane distillation module configurations', *Membranes*, 12(1), p. 81. doi:10.3390/membranes12010081.

Gobran, A.S., Rabie, M., Mohammed, A.H. and Maghrabie, H.M. (2025) 'Technologies, materials, applications, and challenges of membrane distillation: A comprehensive review', *Journal of Industrial and Engineering Chemistry*. doi:10.1016/j.jiec.2025.11.007.

Hu, Y., Chen, G., Huang, M., Qiao, J. and Yang, X. (2025) 'Heat-mass transfer and energy efficiency in direct contact membrane distillation: Effects of membrane properties, temperature, and salt concentration', *Journal of Membrane Science*, p. 124533. doi:10.1016/j.memsci.2025.124533.

Hussain, A., Janson, A., Matar, J.M. and Adham, S. (2022) 'Membrane distillation: Recent technological developments and advancements in membrane materials', *Emergent Materials*, 5(2), pp. 347–367. doi:10.1007/s42247-020-00152-8.

Jing, L., Sun, J., Zhang, Y., Chen, J. and Guo, F. (2025) 'Experimental investigation of temperature polarization near membrane surface during air gap membrane distillation processes', *Membranes*, 15(6), p. 185. doi:10.3390/membranes15060185.

Kharraz, J.A., Bilad, M. and Arafat, H.A. (2015) 'Flux stabilization in membrane distillation desalination of seawater and brine using corrugated PVDF membranes', *Journal of Membrane Science*, 495, pp. 404–414. doi:10.1016/j.memsci.2015.08.039.

Lawson, K.W. and Lloyd, D.R. (1997) 'Membrane distillation', *Journal of Membrane Science*, 124(1), pp. 1–25. doi:10.1016/S0376-7388(96)00236-0.

Lee, J.-Y. (2025) 'Derivation of full range vapor pressure equation from an arbitrary point', *Chemical Engineering Communications*, 212(2), pp. 250–259. doi:10.1080/00986445.2024.2409171.

Lou, J., Vanneste, J., DeCaluwe, S.C., Cath, T.Y. and Tilton, N. (2019)
"Computational fluid dynamics simulations of polarization phenomena in direct contact membrane distillation"

Lou, J., Vanneste, J., DeCaluwe, S.C., Cath, T.Y. and Tilton, N. (2019) 'Computational fluid dynamics simulations of polarization phenomena in direct contact membrane distillation', *Journal of Membrane Science*, 591, p. 117150. doi:10.1016/j.memsci.2019.05.074.

Musie, W. and Gonfa, G. (2023) 'Fresh water resource, scarcity, water salinity challenges and possible remedies: A review', *Heliyon*, 9(8). doi:10.1016/j.heliyon.2023.e18685.

Nthunya, L.N. and Mamba, B.B. (2025) 'Membrane distillation for water desalination: Assessing the influence of operating conditions on the performance of serial and parallel connection configurations', *Membranes*, 15(8), p. 235. doi:10.3390/membranes15080235.

Qasim, M., Samad, I.U., Darwish, N.A. and Hilal, N. (2021) 'Comprehensive review of membrane design and synthesis for membrane distillation', *Desalination*, 518, p. 115168. doi:10.1016/j.desal.2021.115168.

Qtaishat, M., Matsuura, T., Kruczek, B. and Khayet, M. (2008) 'Heat and mass transfer analysis in direct contact membrane distillation', *Desalination*, 219(1–3), pp. 272–292. doi:10.1016/j.desal.2007.05.019.

Salman, M., Ahmed, M., Al-Sairfi, H. and Al-Foudari, Y. (2025) 'Mineral extraction from mixed brine solutions', *Separations*, 12(10), p. 266. doi:10.3390/separations12100266.

Sheikh, M., Fassadi Chimeh, A., Zokaee Ashtiani, F., Fouladitajar, A. and Yavarzadeh, N. (2025) 'Mathematical modeling of direct contact membrane distillation (DCMD) using Knudsen-diffusion model for PVDF membranes', *Journal of Membrane Science and Research*, 11(2). doi:10.22079/jmsr.2025.2040777.1676.

Sherif, M., Liaqat, M.U., Baig, F. and Al-Rashed, M. (2023) 'Water resources availability, sustainability and challenges in the GCC countries: An overview', *Heliyon*, 9(10). doi:10.1016/j.heliyon.2023.e20543.

Soumbati, Y., Bouatou, I., Abushaban, A., Belmabkhout, Y. and Necibi, M.C. (2025) 'Review of membrane distillation for desalination applications: Advanced modeling, specific energy consumption, and water production cost', *Journal of Water Process Engineering*, 71, p. 107296. doi:10.1016/j.jwpe.2025.107296.

Suleman, M., Asif, M. and Jamal, S.A. (2021) 'Temperature and concentration polarization in membrane distillation: A technical review', *Desalination and Water Treatment*, 229, pp. 52–68. doi:10.5004/dwt.2021.27398.

Swaidan, B., Ali, M.I.H., Ali, K., Al-Rub, R.K.A. and Arafat, H.A. (2024) 'A computational fluid dynamics study on TPMS-based spacers in direct contact membrane distillation modules', *Desalination*, 579, p. 117476. doi:10.1016/j.desal.2024.117476.

Taamneh, Y. and Bataineh, K. (2017) 'Improving the performance of direct contact membrane distillation utilizing spacer-filled channel', *Desalination*, 408, pp. 25–35. doi:10.1016/j.desal.2017.01.004.

Wu, H.Y., Wang, R. and Field, R.W. (2014) 'Direct contact membrane distillation: An experimental and analytical investigation of the effect of membrane thickness upon transmembrane flux', *Journal of Membrane Science*, 470, pp. 257–265. doi:10.1016/j.memsci.2014.06.002.

Xu, D., Zhu, Z. and Li, J. (2022) 'Recent progress in electrospun nanofibers for the membrane distillation of hypersaline wastewaters', *Advanced Fiber Materials*, 4(6), pp. 1357–1374. doi:10.1007/s42765-022-00193-0.

Zaragoza, G., Andrés-Mañas, J. and Ruiz-Aguirre, A. (2018) 'Commercial scale membrane distillation for solar desalination', *NPJ Clean Water*, 1(1), p. 20. doi:10.1038/s41545-018-0020-z.